# Supporting Information for: Correlated Axion-Sector Islands in an LVS-Based Multi-Axion Effective Ensemble

Ario Jafari
Department of Physics, Chemistry and Biology (IFM), Linköping University
Linköping, 58183, Sweden
ario.jafari@liu.se

## S1. Ensemble construction and observable provenance

The numerical construction uses the same LVS-based multi-axion effective ensemble described in the main article. Each record contains a positive-definite kinetic matrix, integer instanton charges, instanton curvature amplitudes, photon and gluon anomaly vectors, LVS proxy parameters and initial displacements. Canonical normalization and mass-matrix diagonalization then determine the dark-energy-like direction, visible-state direction, effective decay constants, mass eigenvalues, visible anomaly projections, dark/visible separation diagnostic and lifetimes.

Supporting Information Table S1 separates sampled effective inputs from computed observables and proxy diagnostics.

Table S1: Sampled inputs, computed observables and proxy diagnostics in the LVS-based multi-axion effective ensemble.

| Quantity | Treatment |
|---|---|
| Axion kinetic matrix $K^{\mathrm{ax}}_{AB}$ | sampled effective input |
| Canonical normalization | computed from $K^{\mathrm{ax}}_{AB}$ |
| Canonical mass matrix | computed from $K^{\mathrm{ax}}_{AB}$, $Q$, and instanton curvature amplitudes |
| $F_v$ | computed from the selected visible eigenvector and canonical normalization |
| $g_{v\gamma\gamma}$ and $g_{vgg}$ | computed from anomaly vectors, $S^{-1}$ and the selected visible eigenvector |
| $\eta_{\mathrm{DV}}$ | computed anomaly-leakage diagnostic |
| Saxion mass hierarchy | LVS scaling proxy hierarchy diagnostic |
| Regions I–IV | correlated phenomenological partition of the survivor cloud |

## S2. Extended-analysis modules outside the defining filter set

The main survivor definition uses the theory-control and phenomenological filters listed in the main cut-flow table. Several additional modules can be attached to the same survivor records without changing that definition. Supporting Information Table S2 lists these modules.

Table S2: Extended-analysis modules associated with the LVS-based multi-axion effective ensemble. The defining filter set uses the computed observables and proxy consistency checks listed in the main cut-flow table and the provenance table.

| Item | Status |
|---|---|
| Early-dark-energy fraction | assigned to extended cosmological likelihood studies |
| $\Delta N_{\mathrm{eff}}$ | assigned to extended radiation-sector analyses |
| Saxion Hessian stability | represented by the LVS saxion-proxy hierarchy criterion |
| Strict temperature-dependent QCD-like mass–decay relation | assigned to a dedicated QCD-axion specialization |
| Temperature-dependent relic-density calculation | assigned to relic-density extensions |
| Defect-network gravitational-wave spectra | assigned to defect-network and cosmological-history extensions |
| Explicit global compactification consistency | assigned to geometry-specific compactification construction |

## S3. Uncluttered visible-state projection

The main article shows the visible-state mass–coupling plane together with representative phenomenological overlays. Supporting Information Fig. S1 gives the same final-survivor projection without the overlay elements, making the internal Region I–IV structure and representative points easier to inspect.

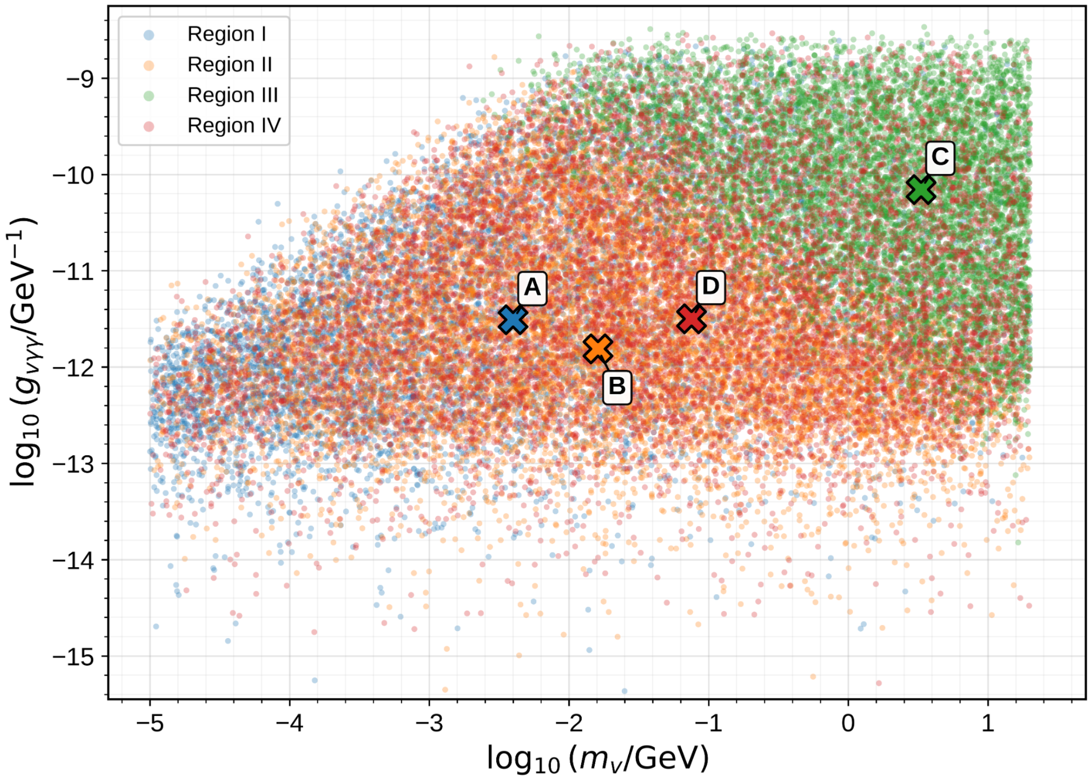


Figure S1: Uncluttered computed visible-state mass–coupling projection for final survivors. The plot shows the internal visible-sector ALP observable plane of the LVS-based multi-axion effective ensemble, with final survivors grouped by Region I–IV and representative final-survivor points A–D marked.

## S4. Robustness and ablation details

The robustness analysis varies the late-time equation-of-state window, visible lifetime threshold, visible photon-coupling window, saxion-control threshold, random seed and prior range. Supporting Information Table S3 gives the numerical details supporting the robustness summary reported in the main text.

Table S3: Robustness grid for the correlated-region structure. Standard cut, seed and prior-range variations preserve populated Region I–IV structures; the extreme long-lifetime stress test isolates a long-lived subset and depletes Region III.

| Test | Variant | Status | $N$ | Min. frac. | I | II | III | IV |
|---|---|---|---|---|---|---|---|---|
| final survivor definition | reference final-survivor set | four-region structure populated | 35,123 | 0.184 | 6,468 | 10,940 | 8,186 | 9,529 |
| w0 window | -1.00005 < w0 < -0.990 | four-region structure populated | 34,278 | 0.189 | 6,468 | 10,826 | 8,026 | 8,958 |
| w0 window | -1.0002 < w0 < -0.980 | four-region structure populated | 35,123 | 0.184 | 6,468 | 10,940 | 8,186 | 9,529 |
| absolute wa cut | \|wa\| <= 0.02 | four-region structure populated | 33,665 | 0.192 | 6,468 | 10,850 | 7,987 | 8,360 |
| absolute wa cut | \|wa\| <= 0.10 | four-region structure populated | 35,123 | 0.184 | 6,468 | 10,940 | 8,186 | 9,529 |
| visible lifetime | tau_v > 1 s | four-region structure populated | 18,508 | 0.008 | 5,046 | 8,090 | 147 | 5,225 |
| visible lifetime | tau_v > 1e4 s | long-lifetime stress-test subset | 10,744 | 0.000 | 3,705 | 4,196 | 0 | 2,843 |
| visible photon coupling lower edge | log10 g > -15.0 | four-region structure populated | 35,118 | 0.184 | 6,466 | 10,938 | 8,186 | 9,528 |
| visible photon coupling lower edge | log10 g > -14.5 | four-region structure populated | 35,086 | 0.184 | 6,457 | 10,925 | 8,186 | 9,518 |
| visible photon coupling upper edge | log10 g < -8.5 | four-region structure populated | 35,121 | 0.184 | 6,468 | 10,940 | 8,184 | 9,529 |
| visible photon coupling upper edge | log10 g < -7.5 | four-region structure populated | 35,123 | 0.184 | 6,468 | 10,940 | 8,186 | 9,529 |
| saxion-control threshold | m_sax/H0 > 1e22 | four-region structure populated | 35,123 | 0.184 | 6,468 | 10,940 | 8,186 | 9,529 |
| saxion-control threshold | m_sax/H0 > 1e18 | four-region structure populated | 35,123 | 0.184 | 6,468 | 10,940 | 8,186 | 9,529 |
| random seed | 260616 | four-region structure populated | 3,433 | 0.193 | 661 | 836 | 946 | 990 |
| random seed | 260617 | four-region structure populated | 3,476 | 0.221 | 896 | 893 | 767 | 920 |
| random seed | 260618 | four-region structure populated | 3,525 | 0.178 | 626 | 913 | 880 | 1,106 |
| prior range | narrow_prior | four-region structure populated | 5,950 | 0.208 | 1,539 | 1,612 | 1,239 | 1,560 |
| prior range | wide_prior | four-region structure populated | 2,931 | 0.176 | 517 | 779 | 824 | 811 |

The ablation analysis compares the reference region assignment with controlled modifications of anomaly projections, dark-direction alignment observables, saxion-control information, lifetime information and the assignment rule. Supporting Information Table S4 gives the corresponding counts and adjusted Rand indices.

Table S4: Ablation variants for the correlated-region structure. The full assignment is compared with controlled modifications of anomaly projections, dark-direction alignment observables, saxion-control information, lifetime information and the region-assignment rule. The adjusted Rand index (ARI) measures agreement with the reference region labels.

| Ablation variant | Physical ingredient tested | ARI | I | II | III | IV |
|---|---|---|---|---|---|---|
| Full analysis | Common kinetic-charge-anomaly construction | 1.000 | 6,468 | 10,940 | 8,186 | 9,529 |
| Randomized anomaly vectors | Visible anomaly projection | 0.452 | 6,745 | 11,476 | 8,172 | 8,730 |
| Randomized charge alignments | Dark-direction charge alignment | 0.105 | 6,360 | 10,919 | 9,486 | 8,358 |
| Neutralized saxion-control information | Saxion hierarchy information | 0.626 | 6,391 | 10,900 | 9,552 | 8,280 |
| Neutralized lifetime information | Visible-state lifetime scaling | 0.567 | 6,006 | 12,038 | 8,190 | 8,889 |
| Alternative region assignment | Region-assignment rule | 0.144 | 10,250 | 7,311 | 10,251 | 7,311 |

# S5. LVS anchor records

The anchor records connect selected final survivors to recognizable large-volume structures. Supporting Information Tables S5, S6 and S7 give the template volume forms, structural data and representative effective-record values.

Table S5: LVS anchor templates used to connect the effective ensemble to recognizable large-volume structures.

| Anchor | LVS template | Volume form | Region-level role |
|---|---|---|---|
| A | Swiss-cheese LVS with three blow-up cycles | $\mathcal{V} = \alpha(\tau_b^{3/2} - \lambda_1\tau_1^{3/2} - \lambda_2\tau_2^{3/2} - \lambda_3\tau_3^{3/2})$ | hierarchical kinetic metric and separated dark direction |
| B | Visible local cycle plus hidden instanton cycles | $\mathcal{V} = \alpha\tau_b^{3/2} - \lambda_v\tau_v^{3/2} - \lambda_h\tau_h^{3/2} - \lambda_s\tau_s^{3/2}$ | visible anomaly projection carried by a local cycle |
| C | Fibred LVS with local blow-up cycles | $\mathcal{V} = \alpha\sqrt{\tau_f}\tau_b - \sum_i \lambda_i\tau_i^{3/2}$ | anisotropic kinetic hierarchy and visible-state displacement |
| D | Aligned multi-instanton local-sector template | $\mathcal{V} = \alpha\tau_b^{3/2} - \sum_i \lambda_i\tau_i^{3/2}$ with aligned instanton rows | approximate charge alignment generating a light direction |

Table S6: Structural data for the LVS anchor records. The table displays the kinetic hierarchy, instanton charge rows, electromagnetic and gluonic anomaly vectors, dark-visible separation and saxion-control scale. Complete kinetic matrices and computed observables are recorded in the accompanying anchor data.

| Anchor | Region | $\log_{10}\kappa(K)$ | $Q$ rows | $C_\gamma$ | $C_g$ | $\eta_{\mathrm{DV}}$ | $m_{\mathrm{sax}}/H_0$ |
|---|---|---|---|---|---|---|---|
| A | I | 19.92 | $(-1,+2,-3)$; $(+0,+2,-3)$; $(+3,+0,+3)$ | $(-4,-3,-1)$ | $(+1,+0,+5)$ | 4.09e-10 | 7.92e+51 |
| B | II | 18.25 | $(-1,+1,+0)$; $(-3,+1,+3)$; $(-1,-2,-2)$ | $(-1,-3,+0)$ | $(-1,-3,-5)$ | 3.97e-10 | 2.54e+51 |
| C | III | 22.67 | $(-1,+1,-2)$; $(-3,+2,+0)$; $(-3,-1,+2)$ | $(+1,+0,-1)$ | $(-3,+5,-4)$ | 2.02e-11 | 9.04e+51 |
| D | IV | 18.86 | $(+1,+0,-3)$; $(+3,-1,+0)$; $(+0,-3,+2)$ | $(+1,+4,-4)$ | $(+5,-3,+4)$ | 2.61e-10 | 1.02e+51 |

Table S7: Representative effective records attached to the LVS anchor templates. Each row is an actual final survivor with kinetic, charge, anomaly and saxion-control data recorded in the accompanying anchor files.

| Point | Region | $\mathcal{V}$ | $g_s$ | $F_{\rm DE}$ | $m_{\rm DE}/H_0$ | $m_v$ [GeV] | $g_{v\gamma\gamma}$ | $m_{\rm sax}/H_0$ |
|---|---|---|---|---|---|---|---|---|
| A | I | 1.249e+05 | 0.347 | 1.524 | 0.230 | 3.979e-03 | 3.102e-12 | 7.918e+51 |
| B | II | 8.930e+05 | 0.249 | 0.673 | 0.322 | 1.610e-02 | 1.546e-12 | 2.542e+51 |
| C | III | 8.048e+05 | 0.398 | 0.749 | 0.452 | 3.311e+00 | 6.993e-11 | 9.036e+51 |
| D | IV | 8.816e+04 | 0.175 | 0.695 | 0.808 | 7.543e-02 | 3.179e-12 | 1.019e+51 |

# S6. Saxion and EFT hierarchy diagnostics

The saxion analysis combines representative anchor-level Hessian quantities with full-ensemble proxy hierarchy summaries. Supporting Information Tables S8 and S9 report these diagnostics.

Table S8: Representative saxion Hessian quantities for the LVS anchor records. The table reports the square roots of the controlled canonical Hessian eigenvalues in $H_0$ units, the positivity result and the EFT hierarchy between the Kaluza–Klein scale and the lightest saxion proxy.

| Point | Region | $\log_{10}\sqrt{\lambda_{\rm min}}/H_0$ | $\log_{10}\sqrt{\lambda_2}/H_0$ | $\log_{10}\sqrt{\lambda_3}/H_0$ | Positive | $\log_{10}(m_{\rm sax}/H_0)$ | $\log_{10}(M_{\rm KK}/m_{\rm sax})$ |
|---|---|---|---|---|---|---|---|
| A | I | 51.90 | 51.90 | 55.52 | yes | 51.90 | 4.93 |
| B | II | 51.41 | 51.41 | 55.52 | yes | 51.41 | 4.86 |
| C | III | 51.96 | 51.96 | 56.04 | yes | 51.96 | 4.34 |
| D | IV | 51.01 | 51.01 | 54.54 | yes | 51.01 | 5.92 |

Table S9: Full-ensemble saxion and EFT hierarchy summary by correlated region. The saxion proxy is far above the adopted $m_{\rm sax}/H_0 > 10^{20}$ control threshold throughout the final survivor set, while the Kaluza–Klein and string scales remain ordered above the visible state.

| Region | $N$ | median $\log_{10}(m_{\rm sax}/H_0)$ | 5% $\log_{10}(m_{\rm sax}/H_0)$ | min $\log_{10}(m_{\rm sax}/H_0)$ | median $\log_{10}(M_{\rm KK}/m_{\rm sax})$ | median $\log_{10}(M_s/M_{\rm KK})$ | min $\log_{10}(M_{\rm KK}/m_v)$ |
|---|---|---|---|---|---|---|---|
| I | 6,468 | 52.75 | 50.29 | 49.29 | 4.38 | 0.23 | 13.18 |
| II | 10,940 | 52.74 | 50.33 | 49.30 | 4.38 | 0.23 | 13.26 |
| III | 8,186 | 52.78 | 50.32 | 49.25 | 4.35 | 0.22 | 13.10 |
| IV | 9,529 | 52.73 | 50.28 | 49.30 | 4.39 | 0.23 | 13.13 |